An experimental study on the characteristics of wind-driven surface water film flows by using a multi-transducer ultrasonic pulse-echo technique

Cite as: Phys. Fluids **29**, 012102 (2017); https://doi.org/10.1063/1.4973398
Submitted: 30 August 2016 • Accepted: 15 December 2016 • Published Online: 09 January 2017

Yang Liu, Wen-Li Chen, Leonard J. Bond, et al.

An experimental study on the characteristics of wind-driven surface water film flows by using a multi-transducer ultrasonic pulse-echo technique

Yang Liu,[1] Wen-Li Chen,[1,2] Leonard J. Bond,[1] and Hui Hu[1,a)]
[1]*Department of Aerospace Engineering, Iowa State University, Ames, Iowa 50011-2271, USA*
[2]*School of Civil Engineering, Harbin Institute of Technology, Harbin, 150090 Heilongjiang, China*

(Received 30 August 2016; accepted 15 December 2016; published online 9 January 2017)

An experimental study was conducted to investigate the characteristics of surface water film flows driven by boundary layer winds over a test plate in order to elucidate the underlying physics pertinent to dynamic water runback processes over ice accreting surfaces of aircraft wings. A multi-transducer ultrasonic pulse-echo (MTUPE) technique was developed and applied to achieve non-intrusive measurements of water film thickness as a function of time and space to quantify the transient behaviors of wind-driven surface water film flows. The effects of key controlling parameters, including freestream velocity of the airflow and flow rate of the water film, on the dynamics of the surface water runback process were examined in great details based on the quantitative MTUPE measurements. While the thickness of the wind-driven surface water film was found to decrease rapidly with the increasing airflow velocity, various surface wave structures were also found to be generated at the air/water interface as the surface water runs back. The evolution of the surface wave structures, in the terms of wave shape, frequency and propagation velocity of the surface waves, and instability modes (i.e., well-organized 2-D waves vs. 3-D complex irregular waves), was found to change significantly as the airflow velocity increases. Such temporally synchronized and spatially resolved measurements are believed to be very helpful to elucidate the underlying physics for improved understanding of the dynamics of water runback process pertinent to aircraft icing phenomena. *Published by AIP Publishing.* [http://dx.doi.org/10.1063/1.4973398]

I. INTRODUCTION

Icing is widely recognized as one of the most serious weather hazards to aircraft operations. Aircraft in-flight icing occurs when small, super-cooled, airborne water droplets, which make up clouds and fog, freeze upon impacting onto a surface which allows the formation of ice.[1] The freezing can be completely or partially depending on how rapidly the latent heat of fusion can be released into the ambient air.[2,3] In a dry regime, all the water collected in the impingement area freezes on impact to form *rime ice*.[4] For a wet regime, only a fraction of the collected water freezes in the impingement area to form *glaze ice* and the remaining water runs back and freezes outside the impingement area. Usually rime ice is associated with colder temperatures, below −10 °C, lower liquid water contents (LWCs), and smaller median volumetric diameters of the water droplets in the cloud. Early rime ice accretion usually closely follows the original contour of the airfoil profiles due to the almost instantaneous freezing of the impinging water droplets, and the aerodynamic performance penalties are not as severe as those of glaze ice. Glaze ice is associated with warmer temperatures, above −10 °C, higher liquid water contents, and larger median volumetric diameters.[5] Glaze is the most dangerous type of ice. Because of its wet nature, glaze ice form much more complicated shapes which are difficult to accurately predict, and the resulting ice shapes tend to substantially deform the accreting surface with the formation of "horns" and larger "feathers" growing outward into the airflow.[6] Glaze ice formation will severely decrease the airfoil aerodynamic performance by causing large scale flow separation which produces dramatic increases in drag and decreases in lift.[7] The adhesive strength of glaze ice was also found to be much stronger than that of rime ice;[8] therefore, glaze ice is also much more difficult to remove once built up.

The behavior of unfrozen surface water transport on an accreting ice surface was found to influence the shape of the resulting glaze ice accretion significantly.[9–12] As shown schematically in Fig. 1, driven by the boundary layer airflow over the ice accreting surface, the surface water film flow would become unstable and surface waves may arise at the water/air interface, due to the shear stresses exerted upon the interface by the airflow. While the behavior of surface water transport prior to freezing has a direct impact on the ice shape due to its effect of redistributing the impinging water mass,[13] it can also affect the ice accretion process indirectly through its impact on surface roughness and modification to local convective heat transfer.[4,14–16] Due to lack of knowledge, current ice prediction tools and ice protection system designs for aircraft icing mitigation usually make use of simplified models which ignore many important details of the interactions of three-phase flows (i.e., air, water, and ice) that are responsible for glaze ice formation and accretion.[4,17–21] This simplistic evaluation of surface water transport behavior, which

a)Author to whom correspondence should be addressed. Electronic mail: huhui@iastate.edu.

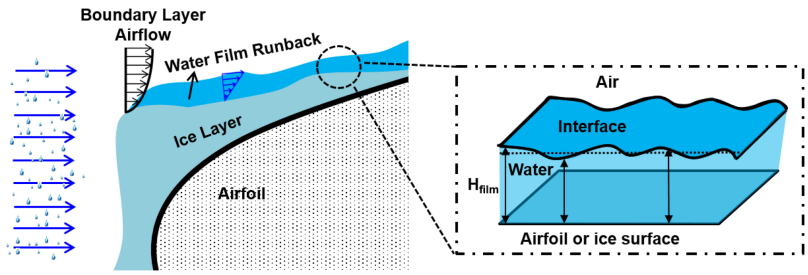

FIG. 1. A schematic of surface water runback over an ice accreting airfoil surface.

omits consideration of the detailed surface physics, is considered to be a significant factor in the poor agreement between the predictions of the current ice accretion models and experimental results for glaze ice accretion process.[4,22–24]

Advancing the technology for safe and efficient aircraft operation in atmospheric icing conditions requires the development of innovative, effective anti-/de-icing strategies tailored for aircraft icing mitigation and protection. Doing so requires a keen understanding of the underlying physics of complicated thermal flow phenomena pertinent to aircraft icing phenomena, both for the ice accretion process itself as well as for the dynamic water runback along the aircraft wing surfaces. The shortage of adequate measurement methods and sensing techniques for aircraft icing physics studies is the bottleneck to limit the efforts. Advanced experimental techniques capable of providing accurate measurements to quantify important microphysical processes are highly desirable to elucidate the underlying physics pertinent to aircraft icing phenomena. In the present study, we report our recent efforts to develop a multi-transducer ultrasonic pulse-echo (MTUPE) technique to achieve temporally synchronized and spatially resolved film thickness distribution measurements to quantify the transient behavior of surface water film flows driven by turbulent boundary layer winds over test plates at different test conditions.

While ultrasonic-based techniques have been widely used as an effective non-destructive testing (NDT) tool to detect internal flaws or structural geometry of solid materials, a number of studies have also been conducted in recent years to use ultrasonic-based techniques to measure surface water/ice thickness for various thermal-fluids applications. Hansman and Kirby[25–27] developed an ultrasonic pulse-echo (UPE) technique to quantify complex multiphase flows (i.e., air, water, and ice) pertinent to aircraft icing phenomena. Serizawa *et al.*[28,29] developed a modified ultrasonic technique to measure local film thickness in a stratified air/water flow over a horizontal plate. Li and Serizawa[30] used a similar method to measure the instantaneous film thickness of a falling film flow in an acrylic resin channel. More recently, Li *et al.*[31] developed an ultrasonic transmission thickness measurement system (UTTMS) to achieve time-resolved film thickness measurements to quantify the behavior of water rivulet/film flows around the surface of a stayed bridge cable suffering from rain-wind induced vibrations.

While ultrasonic-based techniques have been used to quantify complex multiphase flows, most of those previous studies were performed based on pointwise measurements by using a single ultrasonic probe at the point of interest once per time. A common shortcoming of such single point measurements is the incapability of providing spatial correlation of the unsteady water flow structures to effectively reveal the transient behaviors of the surface water transport process. The availability of temporally synchronized and spatially resolved film thickness measurements is highly desirable in order to elucidate underlying physics to improve our understanding about the dynamic surface water runback process pertinent to glaze ice accretion process over aircraft wing surfaces. With this in mind, we developed a multi-transducer ultrasonic pulse-echo (MTUPE) technique to achieve non-intrusive thickness measurements of wind-driven surface water film flows over a test plate as a function of time and space.

While a number of theoretical or/and numerical studies were conducted to investigate the surface water runback process pertinent to glaze ice accretion process over aircraft wing surfaces,[12,21,32] very little can be found in the literature to provide quantitative measurements to characterize the transient behavior of wind-driven surface water film flows. With the MTUPE technique developed in the present study, it will be able to provide temporally synchronized and spatially resolved measurements to characterize the transient behavior of surface water film flows driven by boundary layer airflows. Evolutions of various surface wave structures (i.e., in terms of wave shape, frequency and velocity, and instability modes) generated at the air/water interface could be revealed clearly and quantitatively in both time and space scales. To the best knowledge of the authors, this is the first effort of its kind. The new findings derived from the present study will lead to a better understanding of the important micro-physical processes pertinent to the dynamic water runback process over glaze ice accreting surfaces, which could be used to improve current icing accretion models for more accurate prediction of glaze ice accretion process aircraft wings as well as the development of more effective anti-/de-icing strategies for aircraft icing mitigation.

In the context that follows, the technical basis for the MTUPE technique is introduced at first. Then, the key factors that may influence the resolution and accuracy of MTUPE measurements are discussed. The feasibility and implementation of the MTUPE technique are demonstrated by achieving temporally synchronized and spatially resolved film thickness measurements to quantify the transient behaviors of unsteady surface water film flows driven by turbulent boundary layer winds over a test plate mounted in a low-speed wind tunnel. The effects of the flow controlling parameters, including the flow rate of the surface water flow and the freestream velocity of the airflows, on the dynamics of the wind-driven water film flows over the test plate are evaluated quantitatively based

on the MTUPE measurements. The time series of the film thickness profiles are also formulated to quantify the characteristics of wind-driven surface water film flows and evolution of the surface waves riding on the air/water interfaces.

II. MULTI-TRANSDUCER ULTRASONIC PULSE-ECHO (MTUPE) TECHNIQUE

A. Technical basis of MTUPE technique

The MTUPE system developed in the present study includes a multichannel inspection unit (Omniscan iX, from Olympus NDT Canada, Inc., 1109 78 Ave., Edmonton, Alberta T6P 1L8) and a phased ultrasonic transducer array (i.e., multiple ultrasonic transducers, Part No. V129-RM, bought from Olympus NDT Canada, Inc.). The system is functioned as a multiplexer, which has the capability to simultaneously generate and send voltage pulses to multiple ultrasonic transducers (up to 8 for the system used in the present study). With the high voltage excitation, the ultrasonic transducers can emit ultrasonic waves into the object of interest (i.e., surface water film flows over the test plate). The emitted ultrasonic waves will then interact with different media along their propagation paths and are partially reflected at the interfaces between the different media (e.g., at the interfaces of test plate-water and water-air). The reflected ultrasonic waves are then received by the same transducers in pulse-echoes. These echo responses are collected, recorded, and processed to derive time-resolved film thickness measurements to quantify the transient behavior of the wind-driven surface water film flows over the test plate.

Figure 2 shows schematically the technical basis of the ultrasonic pulse-echo (UPE) technique for achieving quantitative measurements of local water film thickness over a test plate. An ultrasonic pulse is emitted into the surface water film flow over the test plate by using a piezoelectric-based ultrasonic transducer. A fraction of the ultrasonic waves is reflected at the plate-water interface; and the reflected waves, which are identified as the 1st echo, will be received by the ultrasonic transducer in real time. The remaining ultrasonic waves would transmit into the water film flow and then are largely reflected at the water-air interface. The reflected waves, which are identified as the 2nd echo, are partially transmitted through the plate and then received by the transducer. Based on the time-of-flight principle,[33] the local water film thickness can be calculated using following equation:

$$h = (\Delta t \times c)/2, \tag{1}$$

where h is the film thickness, Δt is the time interval between the two echoes, and c is the acoustic velocity in water.

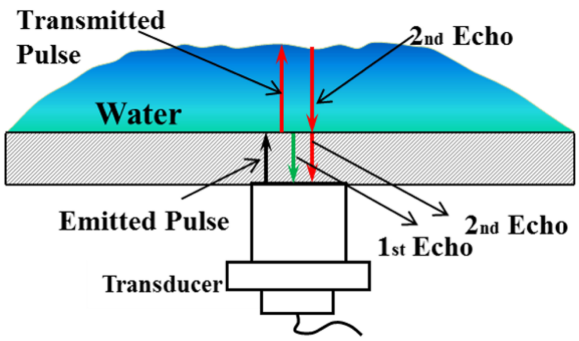

FIG. 2. A schematic to use ultrasonic pulse-echo technique to measure local film thickness.

B. Discussions about the resolution and accuracy of MTUPE measurements

By using UPE technique to measure thickness of a surface water film flow, several key factors need to be considered, which may influence the resolution and accuracy of the UPE measurements. Figure 3(a) shows a typical pulse-echo signal obtained in each channel of a MTUPE system. Several echoes (i.e., in the form of multiple peaks) can be found in the signal sequence. An auto-correlation algorithm (Eq. (2)) is used to determine the time intervals between the echo signals,[34]

$$R(\tau) = \mathrm{E}\left[(Y_t - \mu)(Y_{t+\tau} - \mu)\right] \Big/ \sigma^2, \tag{2}$$

where $R(\tau)$ is the auto-correlation coefficient of the pulse-echo signal as a function of time-lag, τ; Y_t is the signal value for a given run at the time of t, while $Y_{t+\tau}$ is the time-lagged signal value at the time of $t + \tau$. μ and σ are the mean and standard deviation values of the process (Y_t). "E" is the expected value operator.

Figure 3(b) shows an example of the auto-correlation function of the signal sequence. The time intervals between different echoes are determined by finding the time delays corresponding to the local peaks in the auto-correlation profile. As shown clearly in Fig. 3(b), the time interval between the first and second echoes is the time delay at the second correlation peak in the auto-correlation profile. In the real implementation operation, the pulse-echo signal sequence (i.e., Fig. 3(a)) was further processed by filtering out the secondary peaks and digitizing the echo signals with single-pulses. The acquired auto-correlation peaks were found to have a rather small width, i.e., ~0.01 μs.

For UPE measurements, it is also important to match the characteristics of the ultrasonic transducers to the operating configurations. The characteristics of ultrasonic pulse signals emitted by a transducer include near-field fluctuation, beam-spread effect, wave attenuation, mode-conversion, interface reflection, and transmission.[35] In the present study, since the ultrasonic beam was set to be normally incident on the measuring objects, there is a minimal mode conversion at the interfaces. Additionally, since no significant grain or other scatters are embedded along the propagation path of the ultrasonic waves, the wave attenuation is therefore very small and can be neglected. In order to quantitatively evaluate the characteristics of ultrasonic pulse signals, further details about the near field effect, beam spread, and interface reflection and transmission are discussed in the following context.

1. Near field effect

The sound field for a transducer can be generally divided into two zones: near-field and far field. The near-field is the region close to the transducer front where there is an interference between the plane and edge waves going through a series of maxima and minima. As described in the work of Ensminger

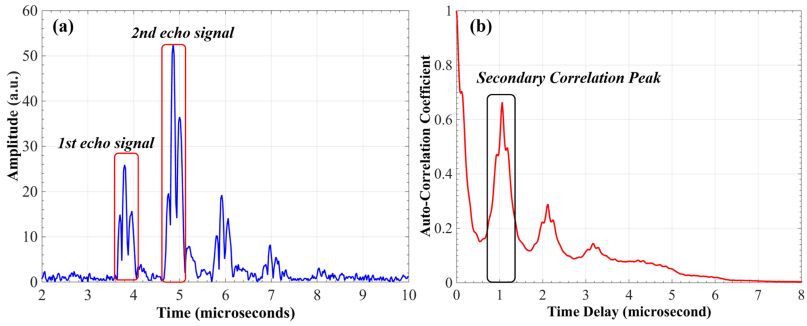

FIG. 3. Typical ultrasonic signals in time-of-flight. (a) A typical signal sequence obtained in each channel of the MTUPE system. (b) Auto-correlation profile of the echo signal.

and Bond,[35] the location of the last maxima is known as the near-field length N_0, which is given by the following equation:

$$N_0 = D^2 f \big/ 4c, \tag{3}$$

where D is element diameter of a transducer, f is the center frequency of the transducer, and c is acoustic velocity.

The far-field is the region beyond the near-field where the wave amplitude on-axis is well behaved and follows a decay/spreading law. Because of the complex acoustic field fluctuation within the near-field, it is usually difficult to make accurate amplitude dependent measurements. Far-field measurements in the range of one to three times of the near field length are generally preferred. For the cases of the present study, the near-field distance was estimated to be less than 7.4 mm based on Equation (3). The region of interest for the present study (>12.5 mm) is therefore beyond the near-field and within the preferred measurement range.

2. Beam spread effect

For a flat ultrasonic transducer with finite aperture, as the ultrasonic beam propagates along the transducer axis, it generally diverges due to the aperture effect, known as "beam spread." Beam spread would take place if the beam is not a perfect cylinder of energy. As particles vibrate, some energy would be transferred radially out of the primary direction of wave propagation.[36] In UPE measurements, "beam-spread" effect may reduce the amplitude of reflections, since the sound field is less concentrated, therefore, becomes less intense within the measurement range. In the present study, the −6 dB pulse-echo beam-spread angle was estimated by using the following equation in order to evaluate the "beam-spread" effect:[35]

$$\sin(\alpha/2) = 0.514c/fD, \tag{4}$$

where $\alpha/2$ is the half angle of spreading between −6 dB points; c is the wave velocity in the media; f is the frequency of the ultrasonic pulse; and D is the diameter of the transducer element.

For the experimental settings used in the present study, the beam spread angle was estimated to be $\alpha = 3.52°$ in the substrate plate and 2.76° in water film. The maximum beam diameters at the plate-water and water-air interfaces were thus estimated to be 0.78 and 0.83 mm, respectively. Then, the beam diameters of the first and second echo signals at the transducer front were estimated to be 1.56 and 1.68 mm, respectively, which are much smaller than the transducer diameter (3.175 mm). Therefore, the energy loss due to the "beam spread" effect is believed to be small and negligible.

3. Interface reflection and transmission

The energy in the ultrasonic pulse-echoes is partitioned at interfaces where there is a difference in acoustic impedance. Since the ultrasonic pulse-echoes would go through two interfaces that generate multiple echo signals, a good estimation of the reflection and transmission is desirable in order to evaluate the signal-to-noise ratio (SNR) of the measurement.

The ratio of the reflected wave amplitude and the incident wave amplitude is known as the reflection coefficient, which can be calculated by using Equation (5). The relationship between the transmission and reflection coefficients at a certain interface is given by Equation (6),

$$R_{12} = R_{21} = \left|(Z_2 - Z_1)/(Z_2 + Z_1)\right|, \tag{5}$$

$$T_{12} \cdot T_{21} = 1 - R_{12}^2, \tag{6}$$

where R_{12} and T_{12} are the acoustic reflection and transmission coefficients at the interface of two different materials (i.e., material #1 and material #2), respectively, when the waves propagate from material #1 to material #2. R_{21} and T_{21} are the acoustic reflection and transmission coefficients at the interface when the waves propagate from material #2 to material #1. Z_1 and Z_2 are the acoustic impedance of the two materials, respectively.

Based on the acoustic properties[35] of the materials used in the present study (as listed in Table I), the reflection coefficients at the plate-water interface and water-air interface were estimated to be 0.32 and 0.99, respectively.

The amplitudes of the 1st echo and the 2nd echo signals were then calculated using the reflection and transmission coefficients, and the results are listed in Table II. By comparing the amplitude of the echo signals with the noise level, the minimum SNR was found to be more than 10 dB for the MTUPE

TABLE I. Acoustic properties of the materials in sound path.

Material	Acoustic speed, c (m/s)	Density, ρ (kg/m^3)	Acoustic impedance, Z (kg/m^2 s ($\times 10^3$))
FullCure®830 VeroWhite	2415	1183	2857
Water (20 °C)	1483	1000	1483
Air (20 °C)	343	1.2	0.412

TABLE II. Estimation of echo amplitude in dB.

Echo signals	Echo amplitude (dB)
1st echo	−5
2nd echo	−1

system with the experimental settings used in the present study. It confirms that the MTUPE system is capable of providing accurate "time-of-flight" measurements with reasonably good SNR for the test cases of the present study.

C. Measurement resolution and validation of the MTUPE system

For the MTUPE system used in the present study, the resolution of the measured water film thickness is determined by the sampling frequency of the system. With the sample rate of the ultrasonic pulses being 100 MHz and the acoustic velocity in water being 1483 m/s at the room temperature of 20 °C, the resolution of the MTUPE system is estimated to be ±7 μm.

An experiment was also designed to demonstrate the feasibility of the MTUPE system described above for water film thickness measurements over a test plate. A pool of water was poured over a flat test plate, and the thickness of the water pool over the test plate was measured by using the MTUPE system. The measurement results of the MTUPE system were compared quantitatively with the nominal thickness (i.e., $h \approx 3.0$ mm) of the water pool. A very good agreement (i.e., difference less than ±10 μm) was found between the nominal water film thickness and the measurement results of the MTUPE system.

D. Experimental setup to quantify wind-driven surface water flows over a test plate

After being carefully calibrated and validated, the MTUPE system was used for achieving temporally synchronized and spatially resolved thickness measurements to quantify the transient behavior of wind-driven surface water film flows over a test plate. The experimental study was conducted in a low-speed open circuit wind tunnel available at Aerospace Engineering Department of Iowa State University. The tunnel has a test section with optically transparent walls, which is 300 mm × 200 mm × 140 mm in length, width, and height, respectively. The wind tunnel has a contraction section upstream of the test section with a set of honeycombs and screen structures installed ahead of the contraction section to provide uniform low turbulent airflow into the test section.[37] The turbulence intensity level in the test section of the wind tunnel was about 1.0%, measured by using a hotwire anemometer.[38]

Figure 4 shows the experimental setup used in the present study to quantify the transient behaviors of wind-driven surface water film flows over a flat test plate, which is used to simulate the dynamic surface water runback over aircraft wing surfaces during glaze ice accretion process. As shown schematically in the figure, the flat test plate, which was designed to be 250 mm in length and 150 mm in width, is made of a hard plastic material (i.e., VeroWhitePlus, RGD835, manufactured by Stratasys, Inc., 5 Fortune Drive, Billerica, MA 01821) by using a rapid prototyping machine (i.e., 3D printer). The upper surface of the test model was processed with fine sandpaper (i.e., up to 2000 grit) and special plastic polishes to achieve a very smooth, glossy finish. During the experiments, the test plate was flush-mounted to the bottom wall of the wind tunnel test section. Two side guide vanes with 4 mm in height and rounded trailing edges were also designed at two sides of the test plate in order to reduce the edge effects to ensure uniform surface water film flows over the test plate.

As shown in Fig. 4, a row of 13 water injection holes with 2.0 mm in diameter was designed over the test plate at a distance of 25.4 mm away from the leading edge of the test plate. During the experiments, a digital gear pump (Cole-Parmer 75211-30) was used to drive water from a reservoir to go through the water injection holes to form a surface water film flow over the test plate. The flow rate of the surface water film flow was controlled by adjusting the settings of the digital gear pump, and monitored by using a digital flowmeter (Omega FLR 1010 T-D). After injected from the water injection holes, the surface water film flow would run back over the test plate, as driven by the boundary layer airflow over the test plate. As

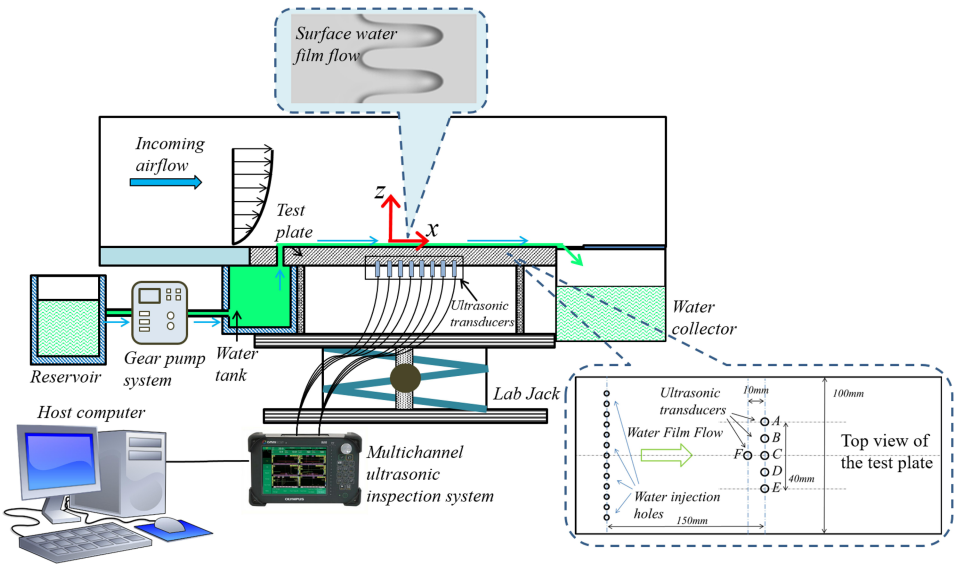

FIG. 4. Experimental setup used to quantify wind-driven surface water film flows.

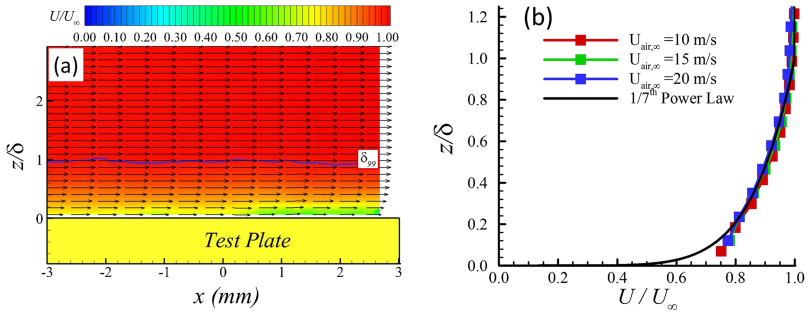

FIG. 5. Time-averaged PIV measurement results of the boundary layer airflow over the test plate without the surface water film. (a) PIV measurement results with $V_{air,\infty}$ = 10 m/s. (b) Measured velocity profiles for the test cases of $V_{air,\infty}$ = 10 m/s, 15 m/s, and 20 m/s, respectively. δ is the boundary layer thickness of the airflow above the test plate.

the wind speed in the wind tunnel becomes high enough (i.e., for the test cases with the freestream wind speed of $U_\infty \geq 10$ m/s), surface waves were found to be generated at the free surface of the surface water film flow at the downstream of the water injection holes.

In order to demonstrate the feasibility and implementation of the MTUPE system described above, an array of 6 ultrasonic transducers, which were mounted at the backside of the flat test plate, were synchronized to measure the thickness of the wind-driven surface water film flow over the test plate. The locations of the ultrasonic transducers were shown schematically in Fig. 4. All of the transducers were connected to the multichannel inspection system (Omniscan iX), which was used to acquire measurement data with a pulse repetition frequency of f_{data} = 1200 Hz.

In the present study, the characteristics of the oncoming boundary layer airflow over the test plate were measured by using a high-resolution Particle Image Velocimetry (PIV) system.[39] Figure 5 shows one example of typical PIV measurement results (i.e., time-averaged velocity profiles) to reveal the characteristics of the turbulent boundary layer airflow over the test plate. It was found that, for the test cases without the surface water film flowing over the test plate, the velocity profiles of the boundary layer airflows were found to follow a 1/7th power law[40] well at the locations where the MTUPE transducers were mounted.

III. MEASUREMENT RESULTS

A. Time-resolved thickness measurements to quantify wind-driven surface water film flows over the flat test plate

As described above, the MTUPE technique is capable of providing time-resolved thickness measurements at multiple points simultaneously to quantify the transient behavior of the wind-driven surface water film flows over the test plate. Figure 6 shows typical measurement results of the MTUPE system in the term of the instantaneous film thickness at the center of the test plate (i.e., at point "C" shown in Fig. 4) with the freestream velocity of the airflow being $V_{air,\infty}$ = 10 m/s and the volumetric flow rate of the surface water film flow changing from Q_{water} = 10 (ml/min)/cm to 30 (ml/min)/cm. While the film thickness measurements were performed at a data acquisition rate of f_{data} = 1200 Hz, only a small portion of the measurement data selected at a much lower sampling frequency was shown in the figure for conciseness.

Based on the time-resolved MTUPE measurements as those shown in Fig. 6, the characteristics of the wind-driven surface water film flow over the test plate were revealed quantitatively. As shown in Fig. 6(a), with the freestream velocity of the airflow being kept as a constant at $V_{air,\infty}$ = 10 m/s, periodical surface waves were found to be generated at the air/water interface, i.e., on the free surface of wind-driven

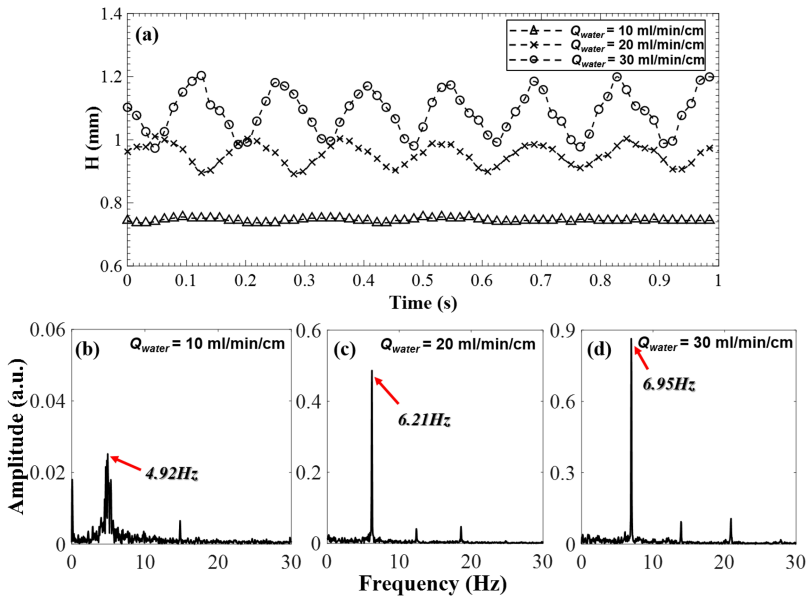

FIG. 6. Time-resolved film thickness measurements at the center of the test plate with the freestream airflow velocity $V_{air,\infty}$ = 10 m/s and water flow rate Q_{water} = 10, 20, and 30 (ml/min)/cm, respectively. (a) Time histories of the measured water film thickness. (b)–(d) are the corresponding power spectra based on the instantaneous film thickness measurements.

water film flow over the test plate. The surface wave structures were found to be two-dimensional for the test cases with the freestream airflow velocity over the test plate being $V_{air,\infty}$ = 10 m/s (i.e., the thickness of the surface waves was found to be quite uniform along spanwise direction, which is revealed from the MTUPE measurement results to be discussed later).

When the volumetric flow rate was set at Q_{water} = 10 (ml/min)/cm, the surface of the water film was found to be rather stable and almost mirror-smooth. The only disturbances to the free surface of the water film flow were the minute waves, which have a frequency of 4.92 Hz, as indicated in the power spectrum shown in Fig. 6(b). These minute waves were suggested to be caused by small fast-moving eddies in the turbulent boundary layer airflow over the surface water film flow, as suggested by Craik.[32] When the volumetric water flow rate was increased to Q_{water} = 20 (ml/min)/cm, along with the increase of film thickness, more obvious sinusoidal surface waves were found to ride on the free surface of the water film flow with a frequency of 6.21 Hz, as shown in Fig. 6(c). As revealed in the previous studies,[11,12,32,41] the surface waves are essentially governed by the shear stresses exerted by the airflow upon the water/air interface, with a normal stress in phase with the wave elevation and a tangential stress in phase with the wave slope. When the stresses are not sufficient to overcome the stiffness of the water film surface due to gravity and/or surface tension, the surface waves can be retained in a stable state.[12,42] As the water flow rate was further increased to Q_{water} = 30 (ml/min)/cm, the surface water film was found to become much thicker, as expected. The surface waves at the free surface of the water film flow were found to develop into a pattern with steeper wave fronts, which are more like triangle waves with a frequency of 6.95 Hz, as shown in the power spectrum plot given in Fig. 6(d). The surface waves were still found to be well-organized, two-dimensional, under the test condition of $V_{air,\infty}$ = 10 m/s and Q_{water} = 30 (ml/min)/cm.

As suggested by Craik[32] and Nelson,[43] a surface water film flow can be considered as a Couette flow. In the present study, the direction of the surface water film flow over the test plate is horizontal (i.e., the flow motion is independent of gravity), and the surface water film flow was driven purely by the shear stresses imposed by the boundary layer airflow. Since the pressure gradient along the airflow direction is negligibly small, i.e., $dp/dx \approx 0$, the transverse velocity profile within the wind-driven water film flows (i.e., a Couette flow with $dp/dx \approx 0$) would be linear, which can be expressed as

$$u(z) = U_{surface} \cdot z/h. \tag{7}$$

As a result, the averaged velocity of the water film flow would be half of the velocity at the free surface of the water film flow, $U_{surface}$. Since the water flow rate, Q_{water}, and the channel width, w, are known, the mean film thickness, h, can be determined based on the MTUPE measurements as those shown in Fig. 6(a), the velocity at the free surface of the water film flow, $U_{surface}$, can be estimated with following equation:

$$U_{surface} = 2Q_{water} \times w/(w \times h). \tag{8}$$

Table III summarizes the measurement results of the wind-driven surface water film flows under some typical test conditions (i.e., freestream velocity of the airflow being $V_{air,\infty}$ = 10 m/s, 15 m/s, and 20 m/s and the water flow rate being Q_{water} = 10 (ml/min)/cm, 20 (ml/min)/cm, and 30 (ml/min)/cm, respectively). The measurement data given in Table III reveal clearly that, even though the freestream velocity of the airflow over the water film flow was kept in constant during the experiments, the runback velocity of the wind-driven water film flow (i.e., as indicated by the free surface velocity, $U_{surface}$) was found to increase greatly as the flow rate of the water film increases. Both the mean thickness and the amplitudes of the surface waves generated at the air/water interface (i.e., as indicated by the standard deviation of the measured film thickness) were also found to increase monotonically with the increasing water flow rate, as expected.

As suggested by Cohen and Hanratty,[44] with the increasing velocity of the airflow, more and more turbulence kinetic energy would be transferred from the airflow to the water film flow as the disturbances at the air/water interface. When the airflow velocity is increased to a high level where turbulence kinetic energy becomes much higher, instability would arise owing to the irreversible kinetic energy transfer from the airflow to the surface disturbances in the forms of various wave patterns. Figure 7 shows the time-resolved measurement results at the center of the test plate with the same water flow rate of Q_{water} = 20 (ml/min)/cm, while the freestream velocity of the airflow over the test plate was changed to $V_{air,\infty}$ = 10 m/s, 15 m/s, and 20 m/s, respectively. The instability transition of the surface waves at the air/water interface with the increasing airflow velocity was revealed clearly based on the film thickness measurement results.

TABLE III. Characteristics of the surface water film flow under some typical test conditions.

$V_{air,\infty}$ (m/s)	Q_{water} ((ml/min)/cm)	Mean film thickness, h (mm)	Standard deviation of the measured film thickness, σ (mm)	Velocity of free surface $U_{surface}$ (mm/s)
10	10	0.745	0.005	44.13
	20	0.960	0.040	68.49
	30	1.090	0.065	90.48
15	10	0.545	0.055	60.32
	20	0.595	0.065	110.50
	30	0.690	0.070	142.93
20	10	0.195	0.035	168.58
	20	0.210	0.050	313.08
	30	0.255	0.065	386.74

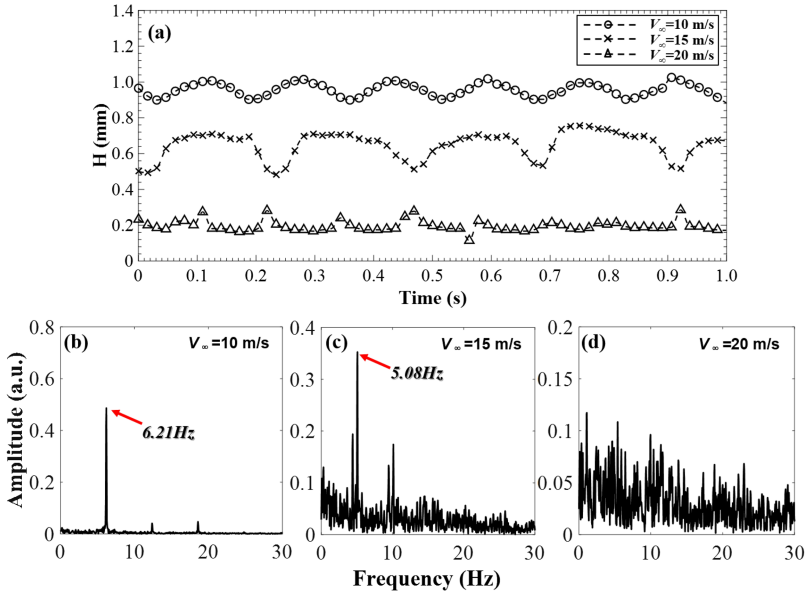

FIG. 7. Film thickness measurement results at the center of the test plate with the same water flow rate of Q_{water} = 20 (ml/min)/cm, but freestream airflow velocity being changed to $V_{air,\infty}$ = 10 m/s, 15 m/s, and 20 m/s, respectively. (a) Time histories of the measured water film thickness; corresponding power spectra of the measured water film thickness at (b)–(d).

As described above, when the freestream velocity of the airflow was kept at a low level, i.e., at $V_{air,\infty}$ = 10 m/s, the wind-driven surface water film flow over the test plate was found to be in a stable state, i.e., rather well-organized, two-dimensional, sinusoidal-shaped surface waves were found to be generated at the free surface of the water film flow. The frequency of the surface waves can be easily identified as the dominant peak frequency in the power spectrum plot of the measured water film thickness (i.e., f_{wave} = 6.21 Hz), as shown clearly in Fig. 7(b). As the freestream velocity of the airflow was increased to $V_{air,\infty}$ = 15 m/s, while the water flow rate still being Q_{water} = 20 (ml/min)/cm, the thickness of the water film was found to become much thinner due to the increased flow velocity of the surface water film driven by the faster airflow. Instead of being smooth, sinusoidal-shaped, the surface waves were found to be featured as pulsed rectangular-shaped waves, i.e., having steep fronts and long rear portions, which have a dominant frequency of f_{wave} = 5.08 Hz, as shown in Fig. 7(c). As the freestream velocity of the airflow was further increased to $V_{air,\infty}$ = 20 m/s, the surface waves were found to become of an obviously non-periodic, random pattern, with no dominant frequency which can be identified in the power spectrum of the measured film thickness data as shown in Fig. 7(d). It indicates that a significant instability change occurred at the air/water interface for the wind-driven surface water film flow over the test plate.

B. Time expansion of spanwise thickness distribution of wind-driven surface water film flows over the flat test plate

Figure 8 gives the time expansion of the simultaneously measured film thickness profiles obtained by using five ultrasonic transducers mounted along the spanwise direction of the test plate, i.e., at points of A, B, C, D, and E as shown in Fig. 4, which can be used to further reveal the characteristics of wind-driven surface water film flows and the instability transition of the surface waves generated at the air/water interface. The measurements were conducted with the same water flow rate of Q_{water} = 20 (ml/min)/cm, while the freestream velocity of the airflow over the test plate was set to be $V_{air,\infty}$ = 10 m/s, 15 m/s, and 20 m/s, respectively. It can be seen clearly that, even though the water flow rate was kept at the same level

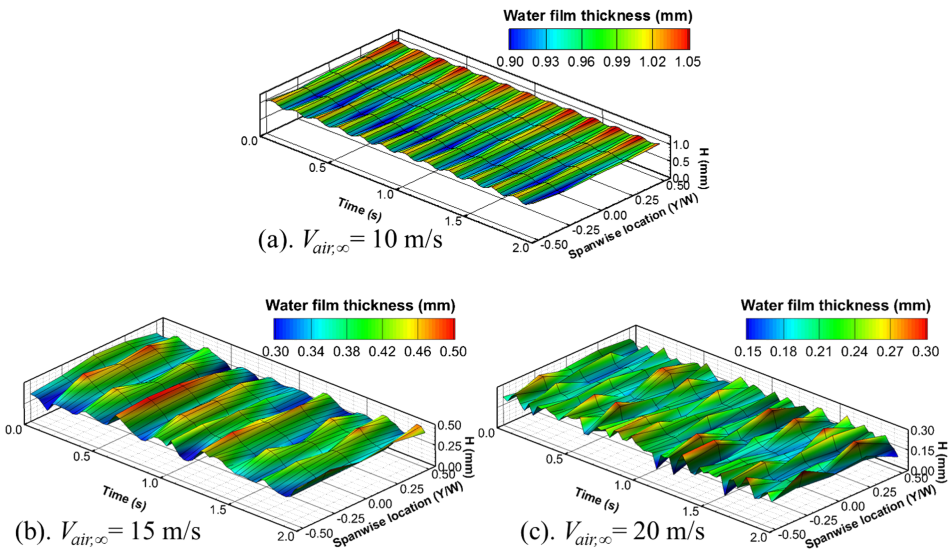

FIG. 8. Time expansion of the simultaneously measured film thickness profiles at the same water flow rate of Q_{water} = 20 (ml/min)/cm, while the freestream airflow velocity being changed to (a) $V_{air,\infty}$ = 10 m/s, (b) $V_{air,\infty}$ = 15 m/s, and (c) $V_{air,\infty}$ = 20 m/s, respectively.

of Q_{water} = 20 (ml/min)/cm, the characteristics of the surface waves generated at the air/water interface for the wind-driven surface water film flow were found to vary significantly as the airflow velocity increases. At first, the film thickness was found to decrease rapidly with the increasing airflow velocity. More specifically, as the freestream velocity of the airflow increases from 10 m/s to 20 m/s (i.e., by a factor of 2.0), the averaged film thickness was found to decrease from 0.96 mm to 0.21 mm (i.e., by a factor of 4.5). Due to the significant reduction of the film thickness for the surface water film flow at a higher airflow velocity, the corresponding Reynolds number of the wind-driven surface water film flow would change greatly, thereby, the viscous dissipation within the surface water film flow can be significantly affected, as suggested by Cohen and Hanratty.[44] In the meantime, the shear stresses exerted by the airflow at the air/water interface will increase as the airflow velocity increases. It would essentially enhance the interaction between the perturbations on the free surface of the water film flow and the turbulent fluctuations in the boundary layer airflow. As a result, instability transition is expected for the surface waves generated at the air/water interface.

As shown in Fig. 8(a), with the freestream velocity of the airflow being kept at a low level, i.e., the test cases of $V_{air,\infty}$ = 10 m/s, well-organized, sinusoidal-shaped waves were found to be formed on the free surface of the wind-driven water film flow. The surface waves generated at the air/water interface were found to be almost two-dimensional, i.e., rather uniform film thickness along the spanwise direction of the test plate. The similar surface wave structures were also observed and called "fast waves" in the experimental study of Craik.[32] Following up of the work of Craik,[32] the wind-driven surface water film flow for such a situation is called in a stable state, and the shear stresses at the air/water interface would be uniformly distributed along the spanwise direction of the test plate. In summary, the wind-driven surface water film flow over the test plate is in a stable state with two-dimensional surface waves generated periodically at the air/water interface when the velocity of the airflow over the surface water film flow is low (i.e., $V_{air,\infty} \leq$ 10 m/s for the present study).

As the freestream velocity of the airflow was increased to $V_{air,\infty}$ = 15 m/s, the magnitude of the turbulent velocity component, thereby, turbulent kinetic energy, in the boundary layer airflow over the surface water film flow would be enhanced. More turbulence kinetic energy would be transferred from the airflow to the surface water film flow. While the thickness of the wind-driven surface water film over the test plate decreased rapidly, the surface waves were found to change from the rather smooth, sinusoidal-shape, as those shown in Fig. 8(a), to the wave shapes with much steeper fronts and longer rear portions, as shown in Fig. 8(b). While the surface waves for this test case were still found to be two-dimensional in general, a number of secondary irregular structures were found to ride on the dominate 2-D wave structures along spanwise direction of the test plate. Since the 2-D feature of the surface wave structures was still the dominate feature for this test case, its frequency can still be identified as the dominant peak frequency in the power spectrum of the measured film thickness data as shown in Fig. 7(c), along with the signatures of the secondary wave structures.

As the airflow velocity was further increased, e.g., $V_{air,\infty}$ = 20 m/s as shown in Fig. 8(c), the magnitude of the turbulent velocity component in the boundary layer airflow over the surface water film flow would become even higher, in comparison with those of the test cases described above. As suggested by Craik[32] and Cohen and Hanratty,[44] due to the irreversible transfer of the turbulent kinetic energy from the airflow to the surface water film flow as the disturbances at the air/water interface, the generation of wave-like structures at the free surface of the wind-driven water film flow over the test plate was found to become much more turbulent and random. As shown in Fig. 8(c), the surface waves at the air/water interface for this test case were found to be no longer two-dimensional anymore but becoming complex three-dimensional structures instead. The transition from periodical two-dimensional waves to complex three-dimensional waves at higher airflow velocity was also observed in the experimental study of Craik,[32] in which different wave patterns were randomly coupled and mixed. Since the generation of the 3-D surface waves at the air/water interface was of obviously non-periodic and random in its nature, no well-defined dominant frequency can be identified in the power spectrum of the film thickness measurement results, as shown in Fig. 7(d). In summary, as the airflow velocity over the wind-driven water film flow was increased to a high level with higher turbulence intensity (i.e., $V_{air,\infty}$ > 15 m/s for the test cases of Q_{water} = 20 (ml/min)/cm described here), the wind-driven surface water film flow over the test plate was found to become rather unsteady with complex three-dimensional surface waves generated randomly at the air/water interface.

Based on the temporally synchronized and spatially resolved film thickness measurements as those given in the present study, the characteristics of the wind-driven surface water film flows over the test plate under different test conditions can be revealed in great detail. Such quantitative measurements are highly desirable to improve our understanding about the transient water runback process over ice accreting surfaces of aircraft wings, which would eventually lead to more accurate prediction of ice accretion on aircraft wings as well as development of effective anti-/de-icing strategies for safer and more efficient operation of aircraft in cold weather.

IV. DISCUSSIONS

As described above and shown in Equation (7), since the transverse velocity profiles within the wind-driven surface water film flows are linear, the shear stresses in the wind-driven surface water film flows can be estimated as

$$\tau_{film} = \mu_{water} \left.\frac{du}{dz}\right|_{z=h} = \mu_{water} \frac{U_{surface}}{h}, \tag{9}$$

where μ_{water} is the viscosity of water.

As shown in Equation (9), the shear stresses in the wind-driven surface water film flows would be a constant for each test case. Since both the velocity of the water film flow at the free surface, $U_{surface}$, and the water film thickness, h, can be determined quantitatively based on the MTUPE measurements, the shear stresses of the wind-driven surface water film

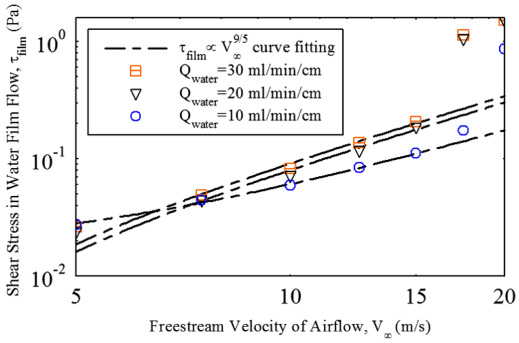

FIG. 9. Measured shear stress in the wind-driven surface water film flow as a function of the freestream velocity of the airflow.

flows can also be estimated for the test cases with different test conditions.

Figure 9 shows the estimated shear stress data of the wind-driven surface water film flows as a function of the freestream velocity of the airflow at different water flow rate levels. It is revealed clearly that, for the test cases with the same water flow rate, the shear stresses of the water film flows would increase gradually with the increasing freestream velocity of the airflow when the freestream airflow velocity is relatively low (i.e., $V_{air,\infty} \le 15$ m/s). The shear stress values were found to increase very rapidly as the freestream airflow velocity becomes much greater (i.e., $V_{air,\infty} > 15$ m/s). The rapid increase of the shear stress was found to correspond well to the occurrence of the instability transition of the surface waves at the air/water interface (i.e., transition from the well-organized 2-D surface waves to complex irregular 3-D wave structures) described above.

According to the Fluid Mechanics textbook of Potter and Wiggert,[45] for a turbulent boundary layer flow over a flat plate, the relationship between the wall shear stress and the freestream velocity of the turbulent flow would follow a scaling law of $V_{air,\infty}^{9/5}$. In the present study, since the shear stress in the wind-driven surface film flow is a constant, the measured shear stress data given in Fig. 9 would also be the shear stresses at the water/airflow interface. Therefore, the fitting curves of the measured shear stress data with the scaling law of $V_{air,\infty}^{9/5}$ were also plotted in Fig. 9 for comparison. It can be seen clearly that, when the wind-driven surface water film flow was found to be in a stable state with well-organized 2-D surface waves generated at the air/water interface at the relatively low freestream airflow velocity of $V_{air,\infty} \le 15$ m/s, the measured shear stress data were found to be well fitted by the scaling law of $V_{air,\infty}^{9/5}$. However, when the wind-driven surface water film flow becames highly unsteady with complex three-dimensional surface wave structures generated randomly at the air/water interface (i.e., for the cases of $V_{air,\infty} \ge 17.5$ m/s), the measured shear stress was found to be greatly under-estimated by the $V_{air,\infty}^{9/5}$ scaling law.

For a wind-driven surface water film flow, as suggested by Ueno and Farzaneh,[21] the growth rate of the disturbances at the air/water interface can be significantly increased as the airflow velocity increases. Since the magnitude of the turbulence intensity of the airflow would be enhanced with the increasing airflow velocity, greater turbulent fluctuations of the shear stresses would exist at the air/water interfaces for the wind-driven water film flows. Tsao[11] and Rothmayer[12] also found that the nonlinear interface motion would be strongly influenced by the shear stresses and pressure gradients from the boundary layer airflows. As a result, the perturbations at the air-water interfaces would easily become unstable,[11] as the freestream velocity of the airflow increases. The dynamic interaction between the perturbations and the turbulent fluctuations in the airflow would give rise to stronger fluctuations of the shear stresses,[32] which may trigger interface instability. In the present study, a new parameter, named boundary slip factor (BSF), is introduced to evaluate the instability transition of the surface waves generated at the air/water interface. The BSF, β, is defined as the ratio of the velocity at the free surface of the water film flow to the freestream velocity of the airflow over the test plate, which is expressed as

$$\beta = U_{surface} \Big/ V_{air,\infty} = 2Q_{water} \times w \Big/ \left(w \cdot \tilde{h} \cdot V_{air,\infty}\right), \qquad (10)$$

where Q_{water} is the water flow rate, w is the width of the surface water film flow, $\bar{h}$ is the averaged water film thickness, and $V_{air,\infty}$ is the freestream velocity of the airflow in the wind tunnel.

Figure 10 shows the variations of the measured BSF values as a function of the freestream velocity of the airflow over the test plate at different volumetric flow rates of the surface water film. It is seen clearly that, for the test cases with the same water flow rate of Q_{water} = 10 (ml/min)/cm, the BSF value would decrease at first as the freestream velocity of the airflow increases from $V_{air,\infty}$ = 5 m/s to $V_{air,\infty}$ = 15 m/s. Since the surface motion of the water film flow is mainly driven by the shear stresses exerted by the boundary layer airflow, the velocity of the wind-driven water film flow becomes much faster as the airflow velocity increases, due to the greater shear stress at the air/water interface at a higher airflow velocity. However, the increase of the flow velocity of the wind-driven surface water film was found not to be proportional to that of the airflow velocity due to the thickness changes of the surface water film flow. As the freestream velocity of the airflow goes beyond $V_{air,\infty}$ = 17.5 m/s, the instability transition of the surface waves would occur, as indicated by the surge (i.e., the rapid increase) of the BSF value. It is believed to be caused by the fact that, as the airflow velocity becomes high enough, the shear stresses exerted by the airflow at the air/water interface would overcome the restoring forces comprised of gravity and/or surface tension. As suggested by Craik,[32] the viscous dissipation would be insufficient to balance the energy transfer

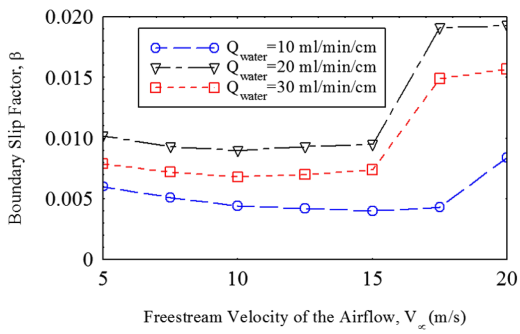

FIG. 10. Variations of the boundary slip factor (BSF) vs. the freestream airflow velocity.

to the corresponding neutral waves, due to which the stable surface wave system would break. As a result, the velocity of the free surface for the surface water film flow over the test plate would increase with a very noticeable change in magnitude.

As shown in Fig. 10, the similar processes were also observed for the test cases with the flow rate of the surface water film being Q_{water} = 20 and 30 (ml/min)/cm. While the corresponding BSF values were still found to decrease at first as the freestream velocity of the airflow increases from $V_{air,\infty}$ = 5 m/s to $V_{air,\infty}$ = 10 m/s, the surge (i.e., the rapid increase) in the BSF values was found to take place at a lower freestream velocity of the airflow as the flow rate of the surface water film flow increases. As shown quantitatively in Fig. 7, the periodic, sinusoidal-shaped surface waves riding on the free surface of the wind-driven water film flow were found to be deformed and eventually turned into non-periodic random structures as the airflow velocity increases to a very high level, indicating the occurrence of the instability transition at the air/water interface. The instability transition at the air/water interface would contribute to the surge (i.e., the rapid increase) in the BSF value, as indicated in Fig. 10.

Figure 11 shows the variations of the time-averaged film thickness of the wind-driven surface water film flow as a function of the freestream velocity of the airflow at different water flow rate levels. It is revealed that, for the test cases with the same water flow rate of Q_{water} = 10 (ml/min)/cm, the time-averaged water film thickness would decrease gradually as the freestream velocity of the airflow increases. As described above, when the airflow velocity is low (i.e., $V_{air,\infty} \leq 15$ m/s for the test cases of the present study), the wind-driven surface water film flow is in a stable state with the surface waves generated at the air/water interface being periodic and almost two-dimensional. As the freestream velocity of the airflow flow was further increased to a higher level (i.e., $V_{air,\infty} > 17.5$ m/s as shown in Fig. 11), the wind-driven surface water film flow was found to become highly unsteady with complex three-dimensional surface waves generated randomly at the air/water interface. A rapid drop of the film thickness was observed for the surface water film flow at $V_{air,\infty} > 17.5$ m/s, which was found to correlate well with the appearance of the surge in the measured BSF value for the water film flow shown in Fig. 10. While a very similar tendency can also be observed for the test cases with higher water flow rate of Q_{water} = 20 and 30 (ml/min)/cm, the rapid drop of the film thickness was found to occur at a lower velocity of the airflow

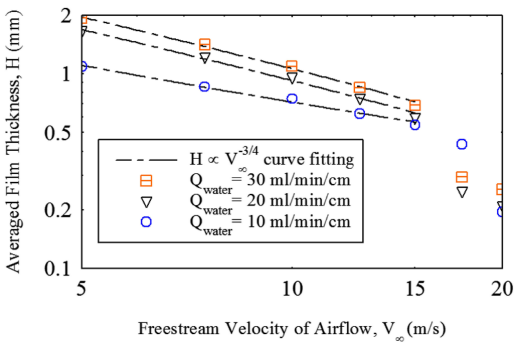

FIG. 11. Averaged film thickness of the wind-driven surface water film flow as a function of the freestream velocity of the airflow.

(i.e., at $V_{air,\infty} \approx 15$ m/s for the test cases of Q_{water} = 20 and 30 (ml/min)/cm vs. at $V_{air,\infty} \approx 20$ m/s for the test cases of Q_{water} = 10 (ml/min)/cm) as shown in Fig. 11.

In an experimental study to characterize the water runback process over an airfoil/wing surface, Anderson and Feo[46] suggested an empirical correlation of the experimentally acquired water film thickness data over the airfoil surface with the liquid water content (*LWC*) of the oncoming airflow and Reynolds number (*Re*) of the test cases. With the assumption of the water runback flow over the airfoil surface being two-dimensional, the best empirical correlation of the experimental film thickness data was found to be

$$h \propto (LWC/\rho_w)^{1/2} Re^{-1/4}. \tag{11}$$

At a specified water flow rate supplied to the oncoming airflow, the liquid water content in the airflow would be inversely proportional to the freestream airflow velocity (i.e., $LWC \propto V_{air,\infty}^{-1}$). The Reynolds number of the test case is proportional to freestream velocity of the airflow (i.e., $Re \propto V_{air,\infty}$). Therefore, the relationship between the water film thickness over the airfoil surface and the freestream airflow velocity can be given as

$$h \propto V_{air,\infty}^{-3/4}. \tag{12}$$

With this in mind, the $V_{air,\infty}^{-3/4}$ scaling law was also used in the present study to fit the measured water film thickness. The fitted curves were also plotted in Fig. 11 for comparison. It can be seen that, when the wind-driven surface water film flow over the test plate was in a stable state, i.e., being almost 2-D, for the test cases of $V_{air,\infty} \leq 15$ m/s, the measured film thickness data were found to be well fitted by the $V_{air,\infty}^{-3/4}$ scaling law. However, when the wind-driven surface water film flow becomes highly unsteady with complex three-dimensional surface wave structures generated randomly at the air/water interface (i.e., for the cases of $V_{air,\infty} \geq 17.5$ m/s), the thickness of the wind-driven surface water film flow was found to be over-estimated greatly by the $V_{air,\infty}^{-3/4}$ scaling law.

V. CONCLUSIONS

In the present study, a multi-transducer ultrasonic pulse-echo (MTUPE) technique was developed and applied to achieve temporally synchronized and spatially resolved thickness measurements to quantify transient behavior of wind-driven surface water film flows pertinent to glaze ice accretion process over aircraft wings. The MTUPE technique is based on a "time-of-flight" principle to achieve non-intrusive water film thickness measurements. Multiple ultrasonic transducers were used to emit ultrasonic pulses simultaneously into surface water film flows over a test plate. While a fraction of the ultrasonic waves was reflected at both the plate/water and water/air interfaces as echoes, the reflected echoes were received by the same ultrasonic transducers in real time. The water film thickness measurements were achieved by multiplying the time delays between the reflected echoes from the plate/water and the air/water interfaces (which can be determined easily based on an auto-correlation operation of the echo signals) with the known propagation velocity of the ultrasonic waves in the water.

After being carefully calibrated and validated, the MTUPE technique was used to achieve time-resolved film thickness measurements to quantify transient behaviors of wind-driven surface water film flow over a test plate. The experimental study was performed in a low-speed wind tunnel with the surface water film flows driven by boundary layer airflows over a test plate to simulate the dynamic water runback processes over ice accreting surfaces of aircraft wings. During the experiments, while the freestream velocity of the airflow over the test plate was changed from $V_{air,\infty} = 5$ m/s to 20 m/s, the volumetric flow rate of the water film was adjusted from $Q_{\text{water}} = 10$ (ml/min)/cm to $Q_{\text{water}} = 30$ (ml/min)/cm. The characteristics of the surface water runback process were found to vary significantly as the airflow velocity and/or the flow rate of the water film changes. While the thickness of the wind-driven water film flow was found to decrease rapidly with the increasing airflow velocity, surface wave structures were also found to be generated at the air/water interface as the surface water runs back. When the airflow velocity is kept at a low level (i.e., $V_{air,\infty} \leq 10$ m/s for the test cases of the present study), the wind-driven water film flow was found to be in a stable state with the surface waves being two-dimensional (i.e., 2-D) and sinusoidal-shaped. As the airflow velocity increases (i.e., at $V_{air,\infty} \approx 15$ m/s for the test cases of the present study), while the sinusoidal-shaped surface waves were found to be deformed to have much steeper fronts and longer rear portions, a number of smaller three-dimensional (i.e., 3-D) wave structures were also found to ride on the dominant 2-D wave structures. With the airflow velocity becoming sufficiently high (i.e., $V_{air,\infty} \geq 17.5$ m/s for the test cases of the present study), the well-organized, 2-D surface wave structures were found to eventually break into many smaller in size but more complex 3-D wave structures. The instability transition of the surface waves for the wind-driven surface water film flows (i.e., transition from having periodically generated large 2-D surface wave structures to having randomly formed complex 3-D wave structures at the air/water interfaces) was found to take place earlier, as the water flow rate of the surface film increases.

It was also found that, when the wind-driven surface water film flow was in a stable state (i.e., having well-organized 2-D surface wave structures at the air/water interface), the relationship between the water film thickness and the airflow velocity was represented well by using an empirical $V_{air,\infty}^{-3/4}$ scaling law, as suggested in previous studies. However, after the instability transition of the wind-driven surface water film flow from 2-D to 3-D (i.e., having complex 3-D irregular wave structures randomly generated at the air/water interface), while the velocity of the surface water film flow was found to increase dramatically, the water film thickness would decrease significantly. As a result, the empirical $V_{air,\infty}^{-3/4}$ scaling law was found to become invalid, i.e., would be over-estimating the film thickness.

To the best knowledge of the authors, this is the first experimental study to provide such detailed, temporally synchronized and spatially resolved measurements to quantify the transient behavior of surface water transport process pertinent to glaze ice accretion process over aircraft wing surfaces. The findings derived from the present study are believed to be essential and very helpful to elucidate the underlying physics for better understanding of the dynamic water runback process pertinent to aircraft icing phenomena, which could be used to improve current icing accretion models for more accurate prediction of glaze ice accretion phenomena as well as for the development of more effective anti-/de-icing strategies to ensure safer and more efficient aircraft operation in cold weather.

ACKNOWLEDGMENTS

The research work is partially supported by National Aeronautical and Space Administration (NASA) Grant No. NNX12AC21A and Iowa Space Grant Consortium (ISGC) Base Program for Aircraft Icing Studies. The support of National Science Foundation (NSF) under Award Nos. of CBET-1064196 and CBET-1435590 is also gratefully acknowledged. Ultrasonic equipment used for the present study is provided through the NSF IU-CRC Center for Nondestructive Evaluation, Iowa State University.

[1] R. W. Gent, N. P. Dart, and J. T. Cansdale, "Aircraft icing," Philos. Trans. R. Soc., A **358**, 2873 (2000).
[2] R. J. Hansman and M. S. Kirby, "Comparison of wet and dry growth in artificial and flight icing conditions," J. Thermophys. Heat Transfer **1**, 215 (1987).
[3] C. Zhang and H. Liu, "Effect of drop size on the impact thermodynamics for supercooled large droplet in aircraft icing," Phys. Fluids **28**, 62107 (2016).
[4] T. G. Myers, J. P. F. Charpin, and C. P. Thompson, "Slowly accreting ice due to supercooled water impacting on a cold surface," Phys. Fluids **14**, 240 (2002).
[5] M. Vargas and J. Tsao, "Observations on the growth of roughness elements into icing feathers," in *45th AIAA Aerospace Sciences Meeting and Exhibit* (American Institute of Aeronautics and Astronautics, Reston, VA, 2007).
[6] S. Campbell, A. Broeren, M. Bragg, and D. Miller, "Aircraft performance sensitivity to icing cloud conditions," in *45th AIAA Aerospace Sciences Meeting and Exhibit* (American Institute of Aeronautics and Astronautics, Reston, VA, 2007).
[7] M. Bragg, G. Gregorek, and J. Lee, "Airfoil aerodynamics in icing conditions," J. Aircr. **23**, 76 (1986).
[8] D. Anderson and A. Reich, "Tests of the performance of coatings for low ice adhesion," AIAA Paper No. 97-0303, presented at the 35th AIAA Aerospace Sciences Meeting and Exhibit, Reno, NV, 1997.
[9] E. Hastings, Jr. and G. Manuel, "Measurements of water film characteristics on airfol surfaces from wind-tunnel tests with simulated heavy rain," in *23rd AIAA Aerospace Sciences Meeting* (American Institute of Aeronautics and Astronautics, Reston, VA, 1985).
[10] E. G. Hill and T. A. Zierten, "Aerodynamic effects of aircraft ground deicing/anti-icing fluids," J. Aircr. **30**, 24 (1993).
[11] J.-C. Tsao, A. P. Rothmayer, and A. I. Ruban, "Stability of air flow past thin liquid films on airfoils," Comput. Fluids **26**, 427 (1997).
[12] A. P. P. Rothmayer, B. D. D. Matheis, and S. N. N. Timoshin, "Thin liquid films flowing over external aerodynamic surfaces," J. Eng. Math. **42**, 341 (2002).
[13] W. Olsen and E. Walker, "Experimental evidence for modifying the current physical model for ice accretion on aircraft surfaces," NASA Tech. Memo. 87184 (Cleveland, OH, USA, 1986).
[14] K. Zhang, T. Wei, and H. Hu, "An experimental investigation on the surface water transport process over an airfoil by using a digital image projection technique," Exp. Fluids **56**, 1 (2015).
[15] Y. Du, Y. Gui, C. Xiao, and X. Yi, "Investigation on heat transfer characteristics of aircraft icing including runback water," Int. J. Heat Mass Transfer **53**, 3702 (2010).
[16] A. P. Rothmayer, K. Zhang, and H. Hu, "Gravitational effects in low-speed air-driven films," in *8th AIAA Atmospheric and Space Environments Conference* (American Institute of Aeronautics and Astronautics, 2016).
[17] W. Wright, *User's Manual for LEWICE Version 3.2* (Cleveland, OH, 2008).
[18] G. Fortin, J.-L. Laforte, and A. Ilinca, "Heat and mass transfer during ice accretion on aircraft wings with an improved roughness model," Int. J. Therm. Sci. **45**, 595 (2006).
[19] B. Thompson and M. Marrochello, "Rivulet formation in surface-water flow on an airfoil in rain," AIAA J. **37**, 45 (1999).

[20]T. G. Myers and C. P. Thompson, "Modeling the flow of water on aircraft in icing conditions," AIAA J. **36**, 1010 (1998).
[21]K. Ueno and M. Farzaneh, "Morphological instability of the solid-liquid interface in crystal growth under supercooled liquid film flow and natural convection airflow," Phys. Fluids **23**, 42103 (2011).
[22]K. Al-Khalil, T. Keith, Jr., and K. De Witt, "Further development of an anti-icing runback model," AIAA Paper No. 91-0266, 1991.
[23]T. G. Myers, "Extension to the Messinger model for aircraft icing," AIAA J. **39**, 211 (2001).
[24]Y. Cao and S. Hou, "Extension to the Myers model for calculation of three-dimensional glaze icing," J. Aircr. **53**, 106 (2016).
[25]R. J. Hansman and M. S. Kirby, "Measurement of ice growth during simulated and natural icing conditions using ultrasonic pulse-echo techniques," J. Aircr. **23**, 492 (1986).
[26]R. J. Hansman and M. S. Kirby, "Measurement of ice accretion using ultrasonic pulse-echo techniques," J. Aircr. **22**, 530 (1985).
[27]R. J. Hansman, M. S. Kirby, R. C. Mcknight, and R. L. Humes, "In-flight measurement of airfoil icing using an array of ultrasonic transducers," J. Aircr. **25**, 531 (1988).
[28]A. Serizawa, K. Nagane, T. Kamei, Z. Kawara, T. Ebisu, and K. Torikoshi, "Dynamic measurement of liquid film thickness in stratified flow by using ultrasonic echo technique," in Proceedings of 4th International Topical Meeting on Nuclear Thermal Hydraulics, Taipei, Taiwan, 2004.
[29]T. Kamei and A. Serizawa, "Measurement of 2-dimensional local instantaneous liquid film thickness around simulated nuclear fuel rod by ultrasonic transmission technique," Nucl. Eng. Des. **184**, 349 (1998).
[30]F.-C. Li and A. Serizawa, "Experimental study on flow characteristics of a vertically falling film flow of liquid metal NaK in a transverse magnetic field," Fusion Eng. Des. **70**, 185 (2004).
[31]F.-C. Li, W.-L. Chen, H. Li, and R. Zhang, "An ultrasonic transmission thickness measurement system for study of water rivulets characteristics of stay cables suffering from wind–rain-induced vibration," Sens. Actuators, A **159**, 12 (2010).
[32]A. D. D. Craik, "Wind-generated waves in thin liquid films," J. Fluid Mech. **26**, 369 (1966).
[33]L. Svilainis, "Review of high resolution time of flight estimation techniques for ultrasonic signals," presented at the 2013 International Conference on NDT, Telford, UK, 8–12 September 2013, pp. 1–12.
[34]Y. Liu, L. J. Bond, and H. Hu, "Reconstruction of wave features in wind-driven water film flow using ultrasonic pulse-echo technique," AIP Conf. Proc. **1706**, 20015 (2016).
[35]D. Ensminger and L. J. Bond, *Ultrasonics: Fundamentals, Technologies, and Applications* (CRC Press, Boca Raton, 2011).
[36]L. W. Schmerr, *Fundamentals of Ultrasonic Nondestructive Evaluation* (Springer US, Boston, MA, 1998).
[37]H. Hu, B. Wang, K. Zhang, W. Lohry, and S. Zhang, "Quantification of transient behavior of wind-driven surface droplet/rivulet flows using a digital fringe projection technique," J. Visualization **18**, 705 (2015).
[38]W. H. Rae and A. Pope, *Low-Speed Wind Tunnel Testing* (John Wiley, 1984).
[39]K. Zhang, Y. Liu, A. P. Rothmayer, and H. Hu, "An experimental study of wind-driven water film flows over roughness array," in *6th AIAA Atmospheric and Space Environments Conference* (American Institute of Aeronautics and Astronautics, 2014).
[40]J. D. Anderson, Jr., *Fundamentals of Aerodynamics* (Tata McGraw-Hill Education, 2010).
[41]D. N. Smyrnaios, N. A. Pelekasis, and J. A. Tsamopoulos, "Boundary layer flow of air past solid surfaces in the presence of rainfall," J. Fluid Mech. **425**, 79 (2000).
[42]C.-S. Yih, "Stability of liquid flow down an inclined plane," Phys. Fluids **6**, 321 (1963).
[43]J. J. Nelson, A. E. Alving, and D. D. Joseph, "Boundary layer flow of air over water on a flat plate," J. Fluid Mech. **284**, 159 (1995).
[44]L. S. Cohen and T. J. Hanratty, "Generation of waves in the concurrent flow of air and a liquid," AIChE J. **11**, 138 (1965).
[45]M. C. Potter and D. C. Wiggert, *Mechanics of Fluids* (Brooks Cole/Thompson Learning, 2002).
[46]D. Anderson and A. Feo, "Ice-accretion scaling using water-film thickness parameters," in *40th AIAA Aerospace Sciences Meeting and Exhibit* (American Institute of Aeronautics and Astronautics, Reston, VA, 2002), AIAA Paper No. 2002-0522.